Journal of Catalysis 290 (2012) 90–100

Contents lists available at SciVerse ScienceDirect

Journal of Catalysis

journal homepage: www.elsevier.com/locate/jcat

Hydrodeoxygenation of *m*-cresol over gallium-modified beta zeolite catalysts

Artit Ausavasukhi [1], Yi Huang, Anh T. To, Tawan Sooknoi *, Daniel E. Resasco *

School of Chemical, Biological and Material Engineering, University of Oklahoma, Norman, OK 73019, USA

ARTICLE INFO

Article history:
Received 25 November 2011
Revised 1 March 2012
Accepted 3 March 2012
Available online 18 April 2012

Keywords:
Ga-doped HBEA
m-Cresol
Deoxygenation
Surface pool mechanism

ABSTRACT

Ga-modified H-Beta (Ga/HBEA) zeolites were evaluated and compared to other Ga-containing catalysts supported on SiO_2 and ZSM-5 (MFI) for the hydrodeoxygenation of *m*-cresol, a model compound representative of lignin-derived phenolics. The products include toluene, benzene, xylene, light hydrocarbons, as well as phenol and other oxygenated compounds. The appearance of bicyclic compounds suggests that the formation of a "surface pool" of oxygenated intermediates may play a role in the reaction pathway. The yield of toluene, a desirable deoxygenated product, increases with reaction temperature, space time (W/F), Ga content, and H_2 partial pressure and depends on the type of support used (Ga/HBEA > HMFI ≫ Ga/SiO_2). The deoxygenation activity of these catalysts seems to depend on the ability of the zeolite to stabilize specific Ga species, for which HBEA is more effective than HMFI and much more than SiO_2.

1. Introduction

Fast pyrolysis is a potential platform for biomass conversion with a number of techno-economic advantages over other processes [1–7]. However, the (bio-oil) obtained by this process includes a complex mixture of oxygen-rich compounds with carbonyl, carboxyl, methoxy, and hydroxyl functional groups that are not suitable for transportation fuels [8–10]. The high oxygen content of bio-oil makes it thermally and chemically unstable, corrosive, and immiscible with hydrocarbons. Therefore, upgrading of bio-oils to fuels necessarily involves deoxygenation [11–15].

Deoxygenation of bio-oil has been typically attempted by using metal-catalyzed hydrotreating [16–19]. It is well known that transition metals are highly active for reactions involving hydrogen (hydrogenation/dehydrogenation and hydrogenolysis). An alternative family of catalysts that can promote hydrodeoxygenation under less severe conditions is that of Ga-doped zeolites. These catalysts are known to exhibit relatively high activity for dehydrogenation and aromatization of light alkane [20–25].

It has been shown that depending on the specific zeolite used as a support, its pretreatment, and loading, Ga may be present in different forms. They include (a) gallium oxide, typically appearing in aggregated form on the external zeolite surface, (b) small particles occluded in the zeolite micropores, and (c) cationic forms, such as oxidic GaO^+, reduced Ga^+, or GaH_2^+ species [26–30]. It is expected that the electro#132;philic nature of such cationic species may enhance the interaction of the catalyst with oxygenated compounds. This enhanced interaction should lead to higher deoxygenation activity in the presence of hydrogen.

In fact, in a recent study, we have shown that Ga-modified HMFI is an effective catalyst for the hydrodeoxygenation of benzaldehyde [31]. In this work, *m*-cresol has been chosen as a model oxygenated compound, representing the many phenolics deriving from the pyrolysis of the lignin fractions in biomass [32]. Ga-doped zeolite catalysts (HBEA and HMFI) and silica-supported Ga were tested as hydrodeoxygenation catalysts for the conversion of *m*-cresol. Different reaction conditions (space time, type of carrier gas, and reaction temperature) have been investigated in a continuous-flow reactor. Temperature-programmed techniques were used to elucidate the nature of the active species and infer possible reaction pathways.

2. Experimental

2.1. Catalyst preparation and characterization

An HBEA zeolite (CP814E, Si/Al ∼ 12.5, from Zeolyst) was impregnated with aqueous solutions of $Ga(NO_3)_3$ to obtain a range of Ga loading (1–6 wt.%). After impregnation, the samples were calcined at 550 °C for 4 h in flow of dry air. Elemental analysis by ICP was conducted to determine the exact compositions (see Table 1). For comparison, two additional samples with 3 wt.% Ga loading were prepared by the impregnation of HMFI (from Sud-Chemie AG, Si/Al ∼ 45) and silica (PPG, Hi-Sil 210), respectively.

Temperature-programmed reduction (TPR) was carried out in a flow system connected to a TCD detector. Prior to the TPR, the sample was heated in dry air for 1 h (30 mL/min) to 550 °C and then cooled to 50 °C. During the subsequent TPR, H_2 consumption

* Corresponding authors. Permanent address: Department of Chemistry, Faculty of Science, King Mongkut's Institute of Technology Ladkrabang, Bangkok 10520, Thailand (T. Sooknoi).

E-mail addresses: kstawan@kmitl.ac.th (T. Sooknoi), resasco@ou.edu (D.E. Resasco).

[1] Permanent address: Program in Applied Chemistry, Rajamangala University of Technology Isan, Nakhon Ratchasima 30000, Thailand.

0021-9517/$ - see front matter © 2012 Elsevier Inc. All rights reserved.
http://dx.doi.org/10.1016/j.jcat.2012.03.003

Table 1
Chemical composition and surface area of catalyst samples.

Catalyst	Si/Al[a]	Ga loading (wt.%)[a]	Surface area (m^2/g)	Density of acid sites[b] (mmol/g)
HBEA	11	–	615	1.20 (1.4)[c]
IGa/HBEA	11	1.0	590	0.94
3Ga/HBEA	11	2.9	580	0.66
6Ga/HBEA	11	5.9	570	0.59
3Ga/SiO_2	–	2.9	370	–
3Ga/HMFI	45	2.8	510	–

[a] Elemental analysis for Si, Al, and Ga by ICP.
[b] As measured by TPD of I PA.
[c] Theoretical acid density calculated from Si/Al ratio.

was recorded as a function of temperature in flow of 2% H_2/Ar (30 mL/min) at a linear heating rate of 10 °C/min.

To quantify the BrØnsted acidity of the samples, temperature-programmed desorption of *i*-propylamine (IPA-TPD) was conducted in a flow system connected to a mass spectrometer (MS). In each measurement, 20 mg of sample was pretreated in flow of He at 550 °C. Alternatively, a few samples were pretreated in flow of H_2 at 550 °C for 2 h. After the pretreatment, the sample was cooled in He to room temperature and consecutive pulses of *i*-propylamine (IPA) were injected onto the sample until saturation (as measured in the MS) was reached. The excess IPA was removed by flowing He. When a constant signal was achieved in the MS, the sample was heated to 900 °C at a rate of 10 °C/min. The mass peaks used to identify the various desorption products were as follows: *i*-propylamine (m/z = 44), propylene (m/z = 41), and ammonia (m/z = 17). The amount of desorbed IPA was simultaneously calibrated with 2 mL pulses of 2% propylene in He, and the BrØnsted acidity was then calculated following the method described by Gorte et al. [33].

2.2. Catalytic activity measurements

The activity of the different catalysts for *m*-cresol conversion was evaluated on a continuous-flow tubular packed-bed reactor. In each run, a stream of 30 mL/min He (or H_2), regulated by a mass flow controller and saturated at 20 °C with *m*-cresol vapor, was used as a feed. The products were periodically collected and analyzed by online gas chromatography (GC). The range of reaction conditions used for these measurements was as follows: 400–550 °C; 1 atm; He or H_2 carrier gas; space time (W/F) 2–22 h.

In addition to the measurements taken in the continuous flow mode, a micropulse reactor was employed to test the amount and reactivity of surface species trapped inside the cages of the zeolite. In these experiments, the reactor was loaded with 0.020 g of catalyst diluted in inert material to get a bed length of 20 mm. As a pretreatment, the catalyst was exposed to H_2 (30 cc/min) at 450 °C for 2 h, then to He (60 cc/min), which was used as the carrier gas for the pulses of 2.3 μmol *m*-cresol. The fraction of *m*-cresol retained by the catalyst in each pulse was measured by an FID detector directly connected at the reactor outlet. Subsequently, pulses of H_2 were sent over the catalyst containing the trapped species. The analysis of the products evolved from these pulses was conducted in a GC/FID. During the time delay between the injection of *m*-cresol and the H_2 pulses, the catalyst was kept under a 60 cc/min He stream. Alternatively, direct analysis of the He stream coming out of the reactor was also performed at a given time after the *m*-cresol injection to determine what products evolve in the absence of added H_2.

2.3. Temperature-programmed decomposition and desorption (TPDD) after reaction

The following TPDD experiment was conducted to characterize the species left on the catalyst surface during reaction. After a typical reaction run over the Ga/HBEA catalyst, the reactor was switched to a flow of He and quickly cooled down to 100 °C. Subsequently, a TPDD was conducted by increasing the temperature from 100 to 900 °C with a heating rate of 10 °C/min, under H_2 as a carrier gas, while monitoring the intensity of the following masses (m/z) in a mass spectrometer: 15 (methane), 18 (water), 27, 41, 56 (hydrocarbons), 78 (benzene), 91 (toluene), 94 (phenol), and 168 (bicyclic compounds).

3. Results

3.1. Catalyst characterization

The characteristics of the catalyst samples, including measured Si/Al ratio, wt.% Ga loading, and BET surface area, are summarized in Table 1. The observed drop in BET area with increasing Ga loading is not very pronounced, indicating that the extent of pore blocking caused by the Ga species was not significant.

The TPR profiles for the five calcined catalyst samples are compared in Fig. 1. For the Ga/HBEA zeolites with low and moderately low Ga loadings, a Gaussian deconvolution of the profiles reveals the presence of several contributions, as previously observed [34]. A single low-temperature reduction peak (~550 °C), present in all the samples, is typically assigned to the reduction in well-dispersed Ga species such as GaO^+ species or small Ga_2O_3 particles interacting with the zeolite. At higher temperatures, a series of reduction peaks (~650–750 °C) are observed. Their position and distribution depend on the Ga content. They are generally attributed to bulk-like Ga_2O_3 particles, separated from or loosely supported on the zeolite matrix. By increasing the Ga loading, the distribution of these peaks shifted to higher temperatures, indicating that, at higher concentrations, the Ga species can further agglomerate into larger Ga_2O_3 clusters, which are more difficult

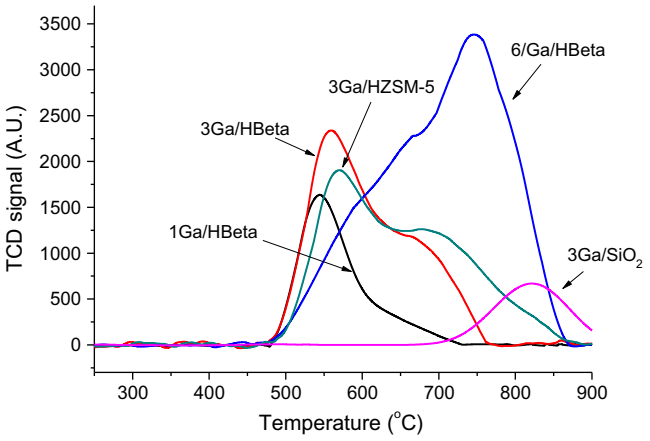

Fig. 1. TPR profiles of (a) 1 Ga/HBEA, (b) 3Ga/HBEA, (c) 6 Ga/HBEA, (d) 3Ga/HZSM-5, (e) 3Ga/SiO_2 after calcination at 550 °C.

to reduce and are expected to be preferentially located on the outer surface of the zeolite [34].

Likewise, the 3Ga/HMFI (Si/Al ~ 45) shows a reduction behavior similar to that of the 3Ga/HBEA sample, with several reduction steps in positions similar to those observed with the Beta zeolite. By contrast, the silica support does not result in a good dispersion of Ga, as evidenced by the appearance of a single broad reduction peak at very high temperature, which can be ascribed to large gallium oxide particles. The lack of any reduction near 550°C indicates the absence of dispersed Ga species, typically observed on the zeolite samples.

The acidity of the HBEA and Ga/HBEA catalysts was determined by the IPA-TPD method [33], and the results are summarized in Fig. 2. The evolution of ammonia and propylene via Hofmann elimination takes place at ~350 °C and provides a direct measurement of the number of bridging BrØnsted acid sites (≡Si—OH—Al≡), strong enough to catalyze this reaction. The densities of BrØnsted acid sites calculated by this method for the different catalysts are included in Table 1. A noticeable decrease in the density of BrØnsted acid sites is observed on the H_2-treated catalysts with increasing loadings of Ga. This trend supports previous suggestions that reduced Ga species (i.e., Ga^+) act as exchangeable cations and replace H^+ BrØnsted sites [30,31,35]. One can compare in Fig. 3 the large relative drop in acid density caused by the addition of Ga compared to the much smaller relative drop in BET surface area. It is clear that the loss of acid density is not due to pore blocking, but rather by the cation exchange.

The observed decrease in acid sites seems to level off at high Ga loadings. That is, the drop in the number of acid sites for the 6 Ga/HBEA zeolite is about the same as that for the 3Ga/HBEA, which only has half as much Ga. To explain this trend, we realize that the latter has most of the Ga species in a high state of dispersion, while the former has a large fraction of the Ga species forming large oxide aggregates outside the zeolite. Therefore, it is reasonable that the exchange of acid sites should be less effective at higher Ga loadings. At the same time, the IPA-TPD shows that the high-Ga-loading zeolite (6 Ga/HBEA) generates new sites that can only decompose IPA at high temperatures (>450 °C). These additional sites with relatively low acid strength have previously been assigned to GaOH species [30,31,35] and may appear only at high Ga loadings.

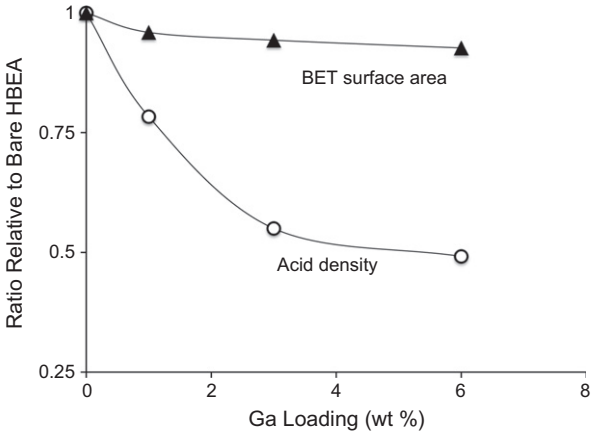

Fig. 3. Effect of Ga loading on relative surface area and acid density as compared to HBEA.

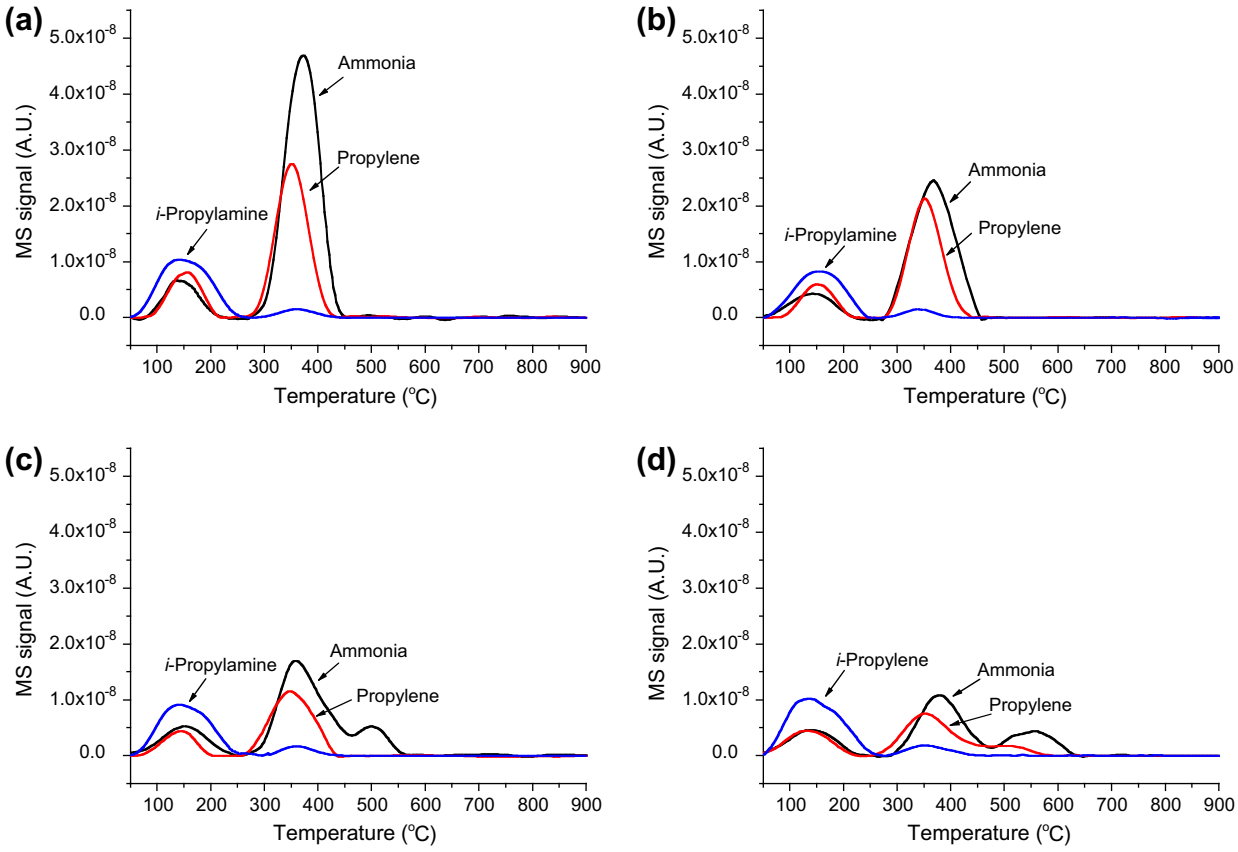

Fig. 2. IPA-TPD of (a) HBEA, (b) red-1 Ga/HBEA*, (c) red-3Ga/HBEA*, (d) 6 Ga/HBeta*. *The Ga-supported zeolite was firstly reduced with H_2 at 550 °C for 2 h and then cooled down to 40 °C under He. Saturation of *i*-propylamine was carried out at 40 °C. The temperature was raised to 900 °C with 10 °C/min under He.

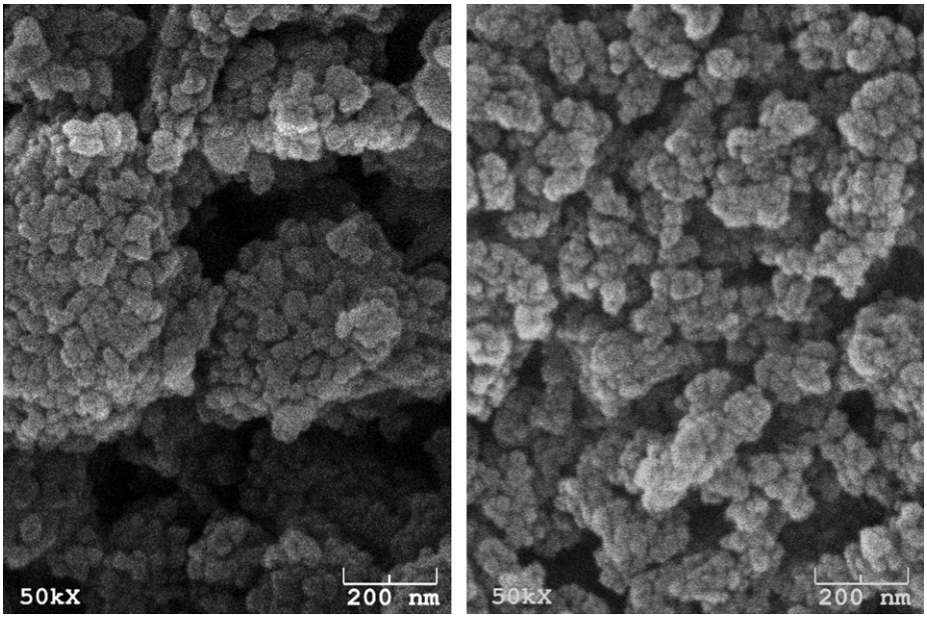

Fig. 4a. SEM images of the 3Ga/HZSM5 (left) and 3Ga/HBeta (right) after calcination.

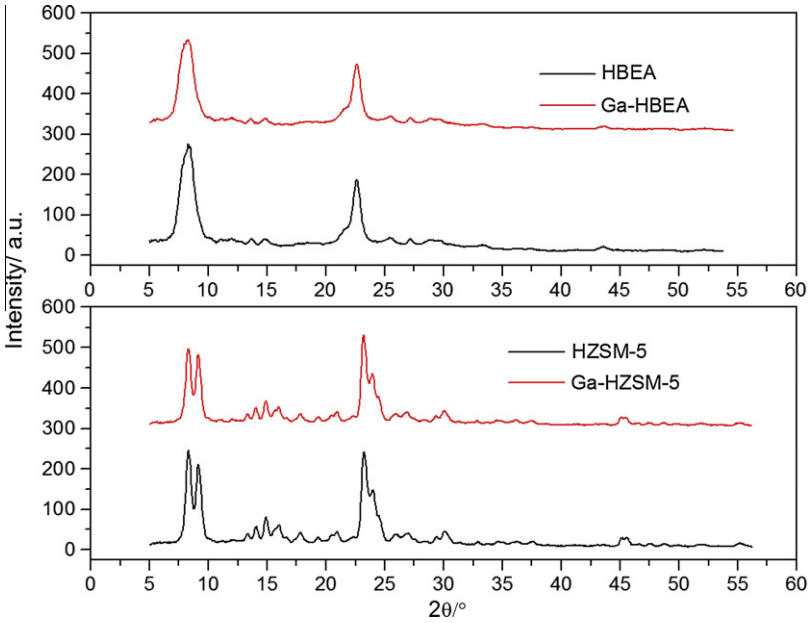

Fig. 4b. XRD analysis of the 3Ga/HZSM5 and 3Ga/HBeta catalysts compared to their corresponding bare H-zeolite.

The reported size of the primary crystals observed by SEM before Ga impregnation is about 20–40 nm for HBEA (Zeolyst, CP814E) and about 50 nm for HMFI (Sud-Chemie, Si/Al = 45) [36]. We have conducted SEM and XRD analysis of the 3Ga/HBEA and 3Ga/HMFI (see Figs. 4a and b). Neither the crystallite size nor the crystallinity shows any significant change upon the incorporation of Ga.

3.2. Catalytic activity

The distribution of products obtained from *m*-cresol conversion in H_2 over 3Ga/HBEA at 400 °C is shown in Fig. 5 as a function of space time (*W*/*F*). A rapid increase in the yields of phenol and heavier phenolic compounds (i.e., bicyclic or oligocyclic substituted phenolics) can be observed when increasing in space time (*W*/*F*) up to about 6 h. A further increase in *W*/*F* results in the decrease in both phenol and oxygenated compounds, while C1, C2—C6 hydrocarbons, benzene, toluene, and xylene slowly increase. The observed evolution of products with *W*/*F* indicates that toluene is not a primary product and that C—OH hydrogenolysis of *m*-cresol to toluene does not occur to a significant extent. The pronounced drop in the yield of the oxygenated compounds observed at intermediate *W*/*F* indicates that these heavier compounds tend to be hydrogenolyzed/decomposed into lighter hydrocarbons as the space time increases. Also, the gradual decline in yield of phenol after *W*/*F* = 6 suggests that phenol can be slowly deoxygenated to hydrocarbons at longer space times.

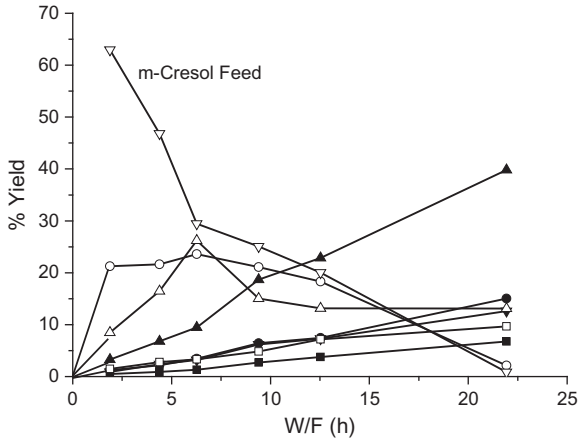

Fig. 5. Effect of W/F over 3Ga/HBeta. Product yield: (■) methane, (●) benzene, (▲) toluene, (▼) xylene, (□) other hydrocarbons, (○) phenol, (Δ) oxygenated compounds. Reaction conditions: Catalyst = 3Ga/HBeta, W/F = 1.9–21.9 h, Reaction temperature = 400 °C, Carrier gas = H_2, Pressure = 1 atm.

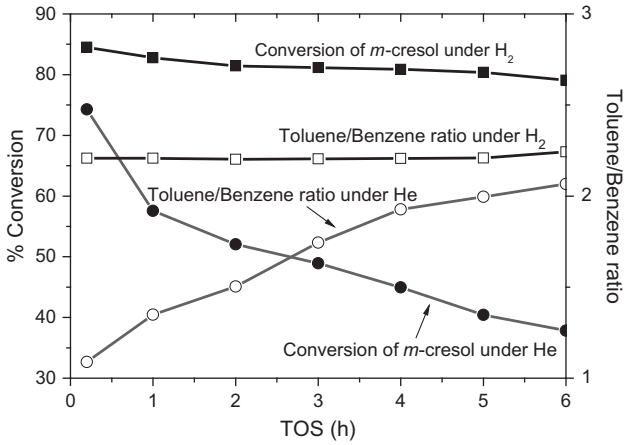

Fig. 6. Effect of carrier gas Reaction conditions: Catalyst = 3Ga/HBeta, W/F = 6.3 h, Reaction temperature = 450 °C, Carrier gas = H_2 or He, Pressure = 1 atm.

As illustrated in Table 2, a very different behavior is observed in the absence of hydrogen. Not only the overall *m*-cresol conversion was lower when using He as a carrier gas instead of H_2, but also the product distribution was very different. While under H_2 deoxygenated hydrocarbons (i.e., benzene, toluene, and xylene) were dominant at high W/F, they were much less important under He at any W/F. Likewise, a significant effect of the carrier gas was observed in the toluene/benzene ratio, which was much higher and stable under H_2 than under He (see Fig. 6). It seems that, under H_2, the C—O bond cleavage to form toluene is relative faster than the dealkylation (C—C cleavage) to form benzene. Without H_2, the toluene/benzene ratio was initially about one but increased as the catalyst deactivated.

The presence of H_2 also has a marked effect on catalyst stability. A rapid deactivation of the catalyst is observed in the absence of H_2, suggesting that high MW intermediates are retained under He carrier gas, but they may be removed in the form of lighter products over the Ga-modified catalysts in the presence of H_2.

The increase in Ga loading had an impact on product distribution. As shown in Table 3, when compared at the same overall conversion and temperature, the increase in Ga content under H_2 resulted in a parallel increase in the production of deoxygenated aromatics at the expense of the high MW oxygenated compounds. It is expected that the C—C and C—O hydrogenolysis activity provided by the incorporation of Ga in the HBEA zeolite results in enhanced formation of benzene, toluene, and methane via hydrogenolysis. Since the density of Brønsted sites decreases with the addition of Ga, we might expect a decrease in cresol conversion as the Ga loading increases. However, as shown in Table 3, the overall conversion does not vary as Ga loading increases from 1 wt.% to 6 wt.%. The absence of conversion drop may indicate that while the addition of Ga reduces Brønsted sites, it may generate Lewis acid sites GaO+ or Ga+, which can still activate cresol at comparable rate. The greatest effect of the addition of Ga is in a drastic increase in the selectivity toward hydrogenolysis products, toluene and benzene, a reaction that is catalyzed by Ga species. At the same time, the selectivity to the heavier oxygenated compounds is

Table 2
Effect of carrier gas.

Reaction condition	Initial		6 h on stream	
	H_2	He	H_2	He
% Conversion	84.52	74.25	79.08	37.84
% Yield				
Methane	2.30	0.36	1.67	0.11
Benzene	10.67	12.89	7.33	0.88
Toluene	23.54	14.03	16.44	1.82
Xylene	10.04	2.56	6.45	0.25
Other hydrocarbon	1.87	3.37	1.36	0.68
Phenol	14.07	22.55	15.72	12.33
Oxygenated compound	22.03	18.49	30.09	21.78
Total yield	84.52	74.25	79.08	37.84
% Selectivity				
Methane	2.72	0.49	2.12	0.28
Benzene	12.62	17.36	9.27	2.32
Toluene	27.85	18.90	20.80	4.80
Xylene	11.88	3.45	8.16	0.67
Other hydrocarbon	2.22	4.54	1.72	1.79
Phenol	16.65	30.36	19.88	32.58
Oxygenated compound	26.06	24.90	38.06	57.56
Total selectivity	100.00	100.00	100.00	100.00
Toluene/benzene ratio	2.21	1.09	2.24	2.07

Reaction condition: Catalyst = 3Ga/HBeta, W/F = 6.3 h,
Reaction temperature = 450 °C, carrier gas = H_2 or He, pressure = 1 atm.

Table 3
Effect of Ga content in the catalyst.

Betazeolite Temperature (°C)	H 450	H 400	1Ga/H 400	3Ga/H 400	6Ga/H 400
% Conversion	70.45	55.51	70.76	70.56	71.64
% Yield					
Methane	0.70	0.87	1.43	1.32	1.55
Benzene	0.80	0.68	3.24	3.45	6.12
Toluene	1.59	2.90	8.74	9.45	21.67
Xylene	0.54	1.38	3.56	3.20	5.40
Other hydrocarbon	2.45	2.83	3.75	3.30	4.80
Phenol	18.22	32.00	19.76	23.61	24.66
Oxygenated compound	46.16	14.83	30.28	26.23	7.44
Total yield	70.45	55.51	70.76	70.56	71.64
% Selectivity					
Methane	0.99	1.58	2.02	1.87	2.17
Benzene	1.14	1.23	4.58	4.89	8.54
Toluene	2.25	5.23	12.35	13.39	30.25
Xylene	0.76	2.49	5.03	4.54	7.53
Other hydrocarbon	3.47	5.10	5.30	4.67	6.70
Phenol	25.86	57.65	27.93	33.45	34.42
Oxygenated compound	65.51	26.71	42.79	37.18	10.39
Total selectivity	100.00	100.00	100.00	100.00	100.00

Reaction condition: $W/F = 6.3$ h,
Reaction temperature = 400 and 450 °C, carrier gas = H_2, pressure = 1 atm.

significantly reduced, indicating that these products are not only produced less by the reduction in Brønsted site density, but also more effectively hydrogenolyzed by the Ga species. To make a more direct comparison, we included in Table 3 the product distribution on the HBEA catalyst at the same overall conversion. It is clear that without Ga, the zeolite produces only small amounts of toluene or benzene, but mostly phenol and condensation compounds.

As shown in Fig. 7, increasing the reaction temperature in the 400–550 °C range not only shows a clear increase in *m*-cresol conversion over 3Ga/HBEA, but also causes significant changes in product distribution. The selectivity to methane, C2—C6 hydrocarbons, benzene, toluene, and xylene increased with temperature, while that to phenol and oxygenated compounds decreased. In fact, this should be the expected trend if, as proposed, the deoxygenated compounds derive from C—O and C—C hydrogenolysis of phenol and other oxygenated compounds. These reactions have relatively high activation energies.

Table 4 compares the product yields obtained over the different catalysts under the same reaction conditions (i.e., $W/F = 6.3$ h, 450 °C, under H_2 flow). Clearly, the Ga/HBEA is the most active catalyst among those investigated in this work. For the same Ga loading, Ga/HBEA is more active than Ga/HMFI and much more than Ga/SiO_2.

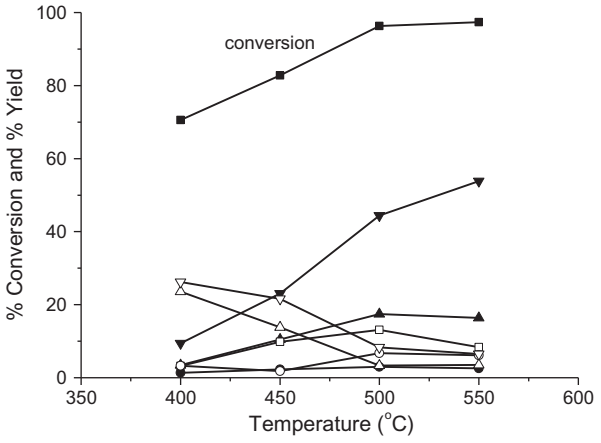

Fig. 7. Effect of temperature yield of (●) methane, (▲) benzene, (▼) toluene, (□) xylene, (○) other hydrocarbons, (Δ) phenol, () oxygenates compounds Reaction conditions: Catalyst = 3Ga/HBeta, $W/F = 6.3$ h, Reaction temperature = 400–550 °C, Carrier gas = H_2, Pressure = 1 atm.

The observed difference in the activity of the two zeolites is most likely related to their different structure. Diffusion of a rather bulky molecule such as *m*-cresol may be more inhibited within the restricted pores of ZSM-5 than in the larger pores of Beta zeolite. As mentioned above, while the crystallite sizes of the two zeolites are not identical, they are very close. The SEM and XRD data in Figs. 4a and b show that the impregnation with Ga and subsequent calcination do not result in crystallinity changes or changes in crystallite size. At the same time, BET measurements show that there are no significant losses in pore volume. Therefore, the transport of reactants and particularly the observed differences in activity between MFI- and BEA-supported catalysts are probably more affected by the zeolite pore size than by the size of the crystallites.

The reason for low conversion and low selectivity to light aromatics obtained on Ga/SiO_2 may be twofold. First, silica is not an effective support for stabilizing highly dispersed Ga species (see TPR results). Second, silica does not contain any significant acidity, which seems to play a role in the conversion of cresol, as evidenced by the relatively high activity exhibited by the Ga-free zeolites (HBEA and HMFI).

3.3. Temperature-programmed decomposition and desorption (TPDD) after reaction

After a period of 6 h under reaction conditions (*m*-cresol/H_2), the decomposition/desorption of the species left on the surface of the 3Ga/HBEA catalyst was conducted by first cooling the catalyst in He to 100 °C and then linearly increasing the temperature to 900 °C under the flow of H_2. As shown in Fig. 8a, the evolution of light aromatics, namely benzene ($m/z = 78$) and toluene ($m/z = 91$), was significant in the 250–450 °C range, together with light hydrocarbons, namely methane ($m/z = 15$) and other hydrocarbons ($m/z = 27, 41, 56$). Above 550 °C, small amounts of high m/z ion fragments ($m/z = 168$) were observed. These heavy fragments are suggested to arise from bicyclic oxygenates, which most probably result from cracking of a surface pool of oxygenated compounds. This cracking (or hydrogenolysis) is accompanied by a significant H_2 consumption and production of water (see Fig. 8b).

3.4. Pulse experiments

To quantify the fraction of *m*-cresol that gets trapped inside the zeolite at 450 °C, a series of *m*-cresol pulses were injected into the He carrier gas of the H_2-pretreated 3Ga/HBEA catalyst. Fig. 9 shows the area count from the FID signal observed at the reactor outlet for a series of 2.3 μmol *m*-cresol pulses injected over a 20-mg catalyst bed. The graph compares the observed signal after the reactor with that observed when the pulses are sent through the bypass. To show more meaningful numbers, the signal is converted to equivalent μmols of *m*-cresol. The important conclusion from this experiment is that it is demonstrated that the Ga/HBEA catalyst traps a large fraction of the *m*-cresol passing through the bed. As more pulses are sent and the catalyst deactivates due to this irreversible adsorption, the amount of species trapped decreases.

Next, to determine whether these trapped species (or surface pool) are reactive intermediates or just deactivating (coke) deposits, we have sent pulses of H_2 over the same sample after connecting the reactor outlet to a GC/FID. The results are summarized in Table 5. Interestingly, no products were evolved upon sending a pulse of H_2 over the sample that was exposed to the entire series of 17 pulses, indicating that this sample was completely deactivated. By contrast, with one *m*-cresol injection, the amount of

Table 4
Effect of support material.

Type of catalyst	3Ga/H Beta	3Ga/Silica	3Ga/H ZSM-5	H ZSM-5
% Conversion	82.78	4.49	40.32	41.69
% Yield				
Methane	2.25	0.78	0.34	1.50
Benzene	10.45	0.15	1.24	1.24
Toluene	23.06	0.32	8.90	2.00
Xylene	9.84	0.00	0.86	0.00
Other hydrocarbon (C2—C6)	1.83	0.00	0.90	1.50
Phenol	13.78	2.82	19.91	23.90
Oxygenated compound	21.57	0.41	8.18	11.55
Total yield	82.78	4.49	40.32	41.69
% Selectivity				
Methane	2.72	17.45	0.84	3.60
Benzene	12.62	3.40	3.08	2.97
Toluene	27.85	7.19	22.06	4.80
Xylene	11.88	0.00	2.13	0.00
Other hydrocarbon (C2—C6)	2.22	0.00	2.23	3.60
Phenol	16.65	62.88	49.38	57.34
Oxygenated compound	26.06	9.08	20.29	27.70
Total selectivity	100.00	100.00	100.00	100.00

Reaction condition: Catalyst = 3Ga/HBeta, 3Ga/Silica, 3Ga/HZSM-5, and HZSM-5, W/F = 6.3 h, reaction temperature = 450 °C, carrier gas = H_2, pressure = 1 atm.

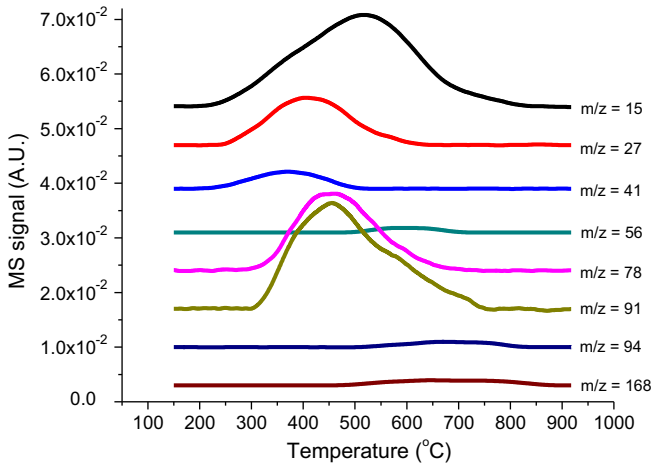

Fig. 8a. TPD of 3Ga/HBeta after *m*-cresol conversion at 400 °C.

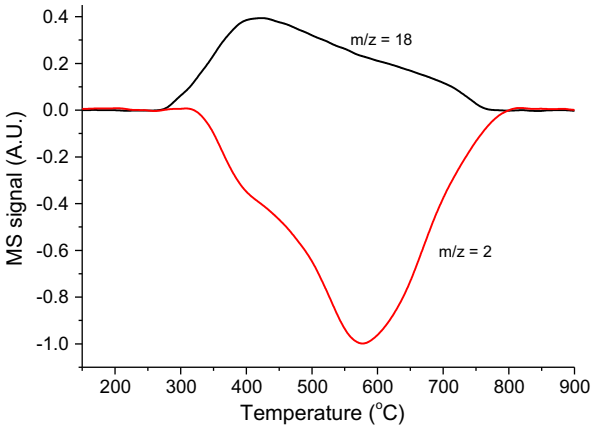

Fig. 8b. TPD of 3Ga/HBeta after *m*-cresol conversion at 400 °C.

products evolved upon sending a subsequent pulse of H_2 was significant, but depended on the time that passed between the *m*-cresol pulse and the subsequent H_2 pulse.

It is important to point out that evolution of deoxygenated products was observed even in the absence of added H_2. That is, when the He stream leaving the reactor was analyzed 5 min after the *m*-cresol injection, benzene, toluene, and xylenes were observed. This product formation suggests that the species trapped inside the zeolite continue reacting under He flow. However, it appears that after 45 min, the surface species either reacted completely or transformed into more refractory surface species since no further product evolution occurred. The results obtained with H_2 pulses indicate that the latter is true. That is, while 60 min after the *m*-cresol injection no product evolution was seen in He, they did appear when we sent a H_2 pulse.

Similarly, as also shown in Table 5, sending a first pulse of H_2 5 min after *m*-cresol injection also yielded the same type of aromatic products, but in significantly larger amounts than seen at the reactor outlet without the addition of H_2. Moreover, when a second H_2 pulse was sent 50 min after the first one, aromatic products were still evolved. These interesting results indicated that the

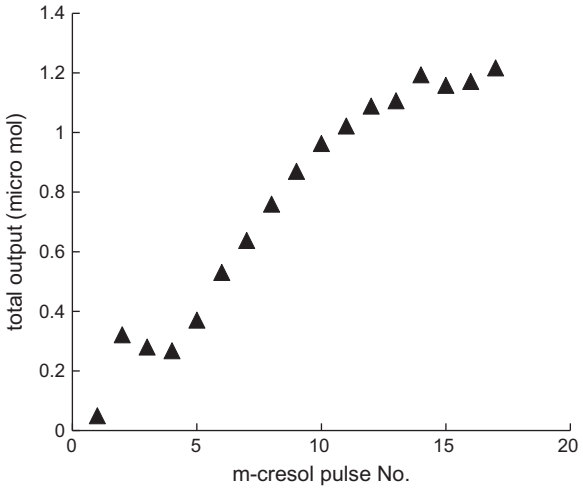

Fig. 9. Total output, expressed as *m*-cresol equivalent, from 17 consecutive pulses of 2.3 μmol *m*-cresol sent over a 20-mg 3Ga/HBEA catalyst at 450 °C.

Table 5
Products evolved at 450 °C from the 3Ga/HBEA catalyst upon the injection of 2.3 μmoles of *m*-cresol followed by H_2 pulses (or not). The time delay indicates the period of time that passed between the *m*-cresol injection and the subsequent injection of H_2 pulse or direct analysis in He, without H_2. During this time, the catalyst was under He flow.

m-cresol exposure (no. of injections)	Time delay in He (min)	H_2 pulse sent (0.5 cc)	Benzene	Toluene	Xylenes	Total products
17	60	Yes	0.0000	0.0000	0.0000	0.0000
1	60	Yes	0.0055	0.0032	0.0000	0.0087
1	5	Yes	0.15	0.18	0.03	0.36
1	55	Yes	0.0039	0.0030	0.0000	0.0069
1	5	No[a]	0.10	0.13	0.02	0.26
1	45	No[a]	0.0000	0.0000	0.0000	0.0000

[a] Direct GC analysis of products in the He stream, without H_2 added.

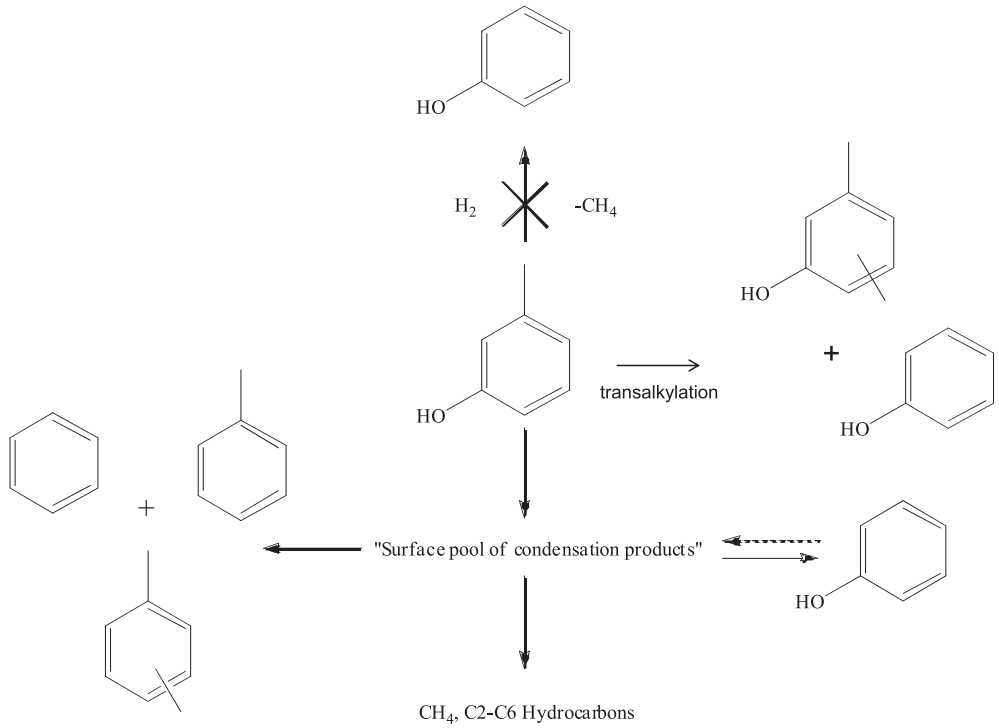

Scheme 1. Reaction pathway for the conversion of *m*-cresol to aromatics, phenol, and trapped surface species.

presence of added H_2 indeed enhances the deoxygenation reaction of the trapped phenolic species, which are unreactive under He.

4. Discussion

Although phenol is the dominant product at low space times, it is not necessarily a primary product formed by direct C—C hydrogenolysis of *m*-cresol to phenol. If that were the case, methane should be produced in equimolar amounts. Therefore, direct dealkylation may only provide a small fraction of the total phenol observed. Alternatively, since *m*-cresol readily adsorbs on the surface of the catalyst, it is possible that a major fraction of the feed gets strongly adsorbed inside the zeolite, forming a "surface pool" of oxygenated species [31]. Similar formation of a surface pool of oxygenates and/or aromatic species trapped inside the nanocages of the zeolite has been proposed to play an important role in determining the product distribution for several zeolite-catalyzed reactions such as MTG [37–40], aromatic disproportionation [41,42], and alkane aromatization [43].

As shown in the TPDD experiments described above, these trapped species can subsequently decompose via cracking or hydrogenolysis at the relatively high temperatures of the experiments to the observed products. In this case, a surface pool of oxygenates would be the primary precursors for phenol and the observed heavy oxygenated compounds. They can also be hydrodeoxygenated, producing the observed light aromatics (benzene, toluene, xylene) and light hydrocarbons (C2—C6 hydrocarbons). As the surface pool intermediate accumulates on the surface, direct dealkylation of the feed (cresol) is further suppressed, leading to the observed decrease in the methane/phenol molar ratio with time on stream (Table 3). By contrast, as recently shown [44,45], acidic zeolites are very effective to catalyze the transalkylation of phenolics and other oxygenated aromatics. Therefore, one can expect that the methyl group from *m*-cresol can be transferred to another aromatic molecule instead of forming methane. In addition, at higher space time, phenol may re-adsorb and undergo further surface condensation in a manner similar to that described for *m*-cresol. This phenomenon was confirmed in a separate experiment using phenol as a feed (not shown) over 3Ga/HBEA, which gave products similar to those observed from *m*-cresol (i.e., benzene, toluene, xylene, and oxygenated compounds). Scheme 1 summarizes the possible products and reaction pathways from *m*-cresol.

One expects that direct cleavage of C—C and C—O bonds does not occur in the absence of hydrogen. However, as shown in Table 5, hydrogenolysis (deoxygenated) products are observed for a short time after injection of *m*-cresol without added H_2. As we have

previously shown [31], the Ga/zeolite catalysts are able to retain hydrogen from a reductive pretreatment, forming $Z^{-}GaH_2^{+}$ species, which themselves react with the trapped surface species forming the observed aromatics. However, this is a temporary effect that disappears after a few minutes in the absence of added hydrogen.

Hence, under He stream, the surface pool of intermediates quickly accumulates and turns into irreversible deposits that lead to coke. While decomposition of the pool leads to the formation of phenol and larger phenolic compounds during some time on stream, a rather rapid catalyst deactivation is observed (Fig 5). That is, H_2 plays an important role in the formation of products via both the direct C—C hydrogenolysis of *m*-cresol and the hydrogenation/hydrogenolysis of the surface pool intermediates. In particular, when H_2 is present, the surface pool intermediates can be removed by hydrogenolysis to lighter aromatic products (benzene and toluene), improving the catalyst stability. The balance between these competing reaction pathways determines whether the catalyst shows stability or deactivates quickly, as described in Scheme 2.

The variation in activity with Ga loading deserves further discussion. It is clear that the yield of light aromatics increased with the Ga content, while the yield of oxygenated compounds decreased (Table 4). The high hydrogenolysis activity of Ga is responsible for this trend, which is also observed at higher reaction temperatures (Fig. 7). Higher temperatures facilitate the decomposition/hydrogenolysis of the surface pool intermediates, leaving more available active sites for consecutive *m*-cresol adsorption and conversion.

As discussed in our previous study [31], the Ga active sites that catalyze the hydrogenolysis of the condensation products of the surface pool are Ga species, only generated under H_2. TPR and

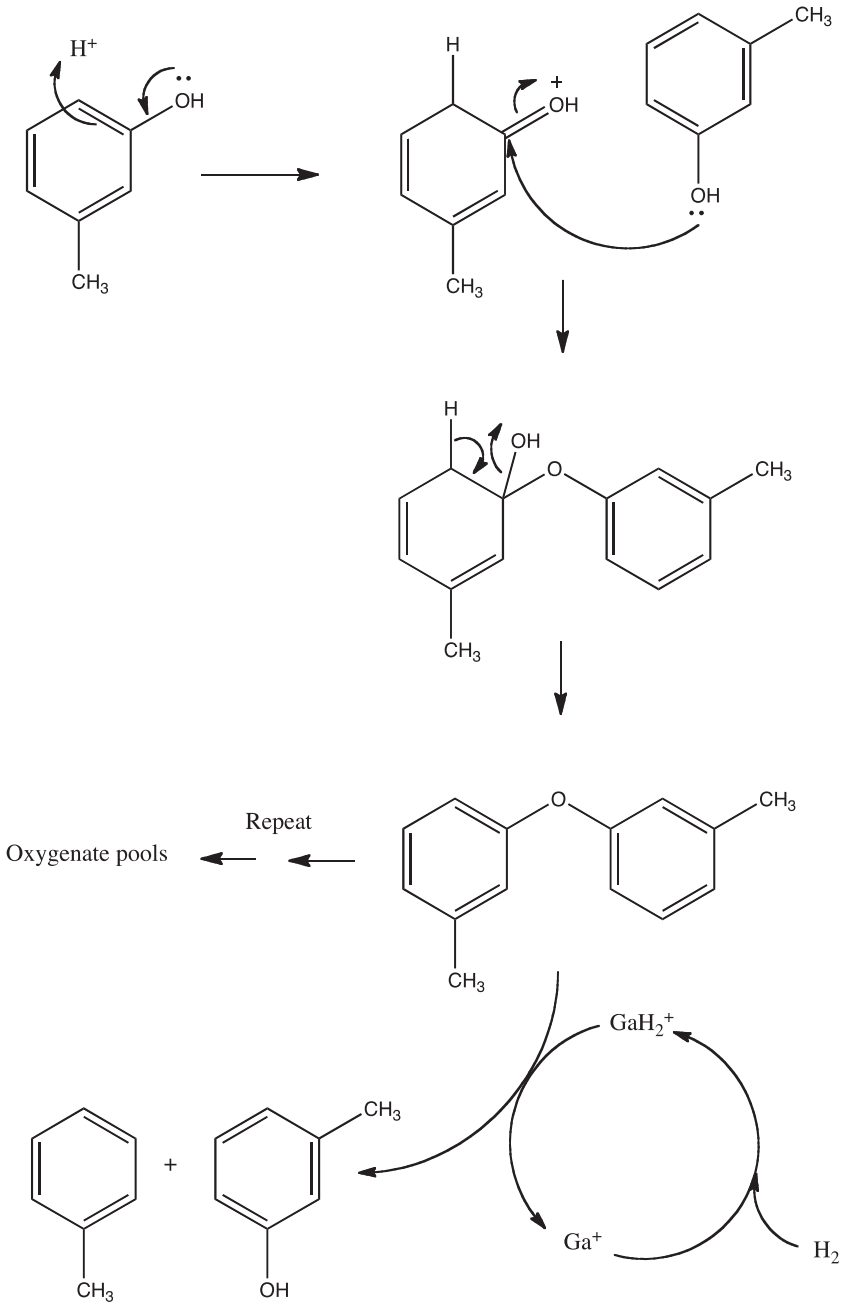

Scheme 2. Possible pathways for the formation of condensed oxygenates that lead to deactivation in parallel to hydrodeoxygenation via formation of GaH_2^{+}species, with hydrogenolysis activity.

IPA-TPD (see Figs. 1 and 2) suggest that reduction in octahedrally coordinated Ga_2O_3 (Ga^{3+} ions) leads to the formation of reduced univalent Ga^+ ions, as previously reported [20,28,46,47], which replace acidic protons.

$$Ga_2O_3 + 2H_2 \rightarrow Ga_2O + 2H_2O \quad (1)$$

$$Ga_2O + 2Z^-H^+ \rightarrow 2Z^-Ga^+ + H_2O \quad (2)$$

where Z^- represents the negative framework charge of the zeolite.Alternatively, these Ga^+ ions can chemisorb molecular H_2 resulting in the formation of gallium dihydrides (GaH_2^+), which have also been proposed as active sites that promote hydrogenolysis [34,46,48,49].

$$Z^-Ga^+ + H_2 \rightarrow Z^-GaH_2^+ \quad (3)$$

The existence of the GaH_2^+ on this type of catalysts has been previously proposed, on the basis of IR absorption bands observed at ~2040 cm^{-1} [30]. Since hydride transfer plays an important role in the formation of light aromatics from phenolics [50,51], we believe that H_2 not only keeps Ga species in its reduced form but can also stabilize GaH_2^+ species, which can promote hydride transfer to the C—C and C—O bond of the condensation product, leading to the formation of lighter aromatics, as discussed above.

In the case of the 3Ga/silica catalyst, it is clear that the inability of silica to stabilize well-dispersed Ga species and promote the formation of gallium dihydrides is responsible for the lack of any hydrodeoxygenation activity (Table 4). Another interesting trend was observed on this catalyst. While the selectivity to phenol was relatively high, there was practically no formation of heavy oxygenated compounds, which appeared in significant amounts on the zeolite catalysts. This difference shows that the formation of the surface pool of condensed intermediates requires the presence of a high density of acid sites as found in zeolites.

The different reactivity exhibited by the Ga-modified HMFI and HBEA zeolites is an interesting matter to discuss. For example, while both 3Ga/HMFI and 3Ga/HBEA stabilize the same type of Ga species and exhibit similar TPR profiles (Fig. 1), the overall *m*-cresol conversion is significantly lower over 3Ga/HMFI than over 3Ga/HBEA. Then, the difference may have a shape-selectivity origin. First, the diffusion of *m*-cresol into the restricted pores of 3Ga/HMFI may be much more constricted than in the pores of 3Ga/HBEA. Second, if as proposed above, the conversion of *m*-cresol involves bimolecular interactions, this reaction path will be hindered inside the structure of 3Ga/HMFI. Therefore, the lower, but still significant activity of 3Ga/HMFI must derive from one of the following possibilities: (i) pore mouth sites or (ii) isomerization of *m*-cresol to a less restricted isomer that can readily diffuse into the pores.

While 3Ga/HMFI results in high selectivity to phenol, methane is not produced at the same rate (Table 4); thus, one cannot conclude that phenol derives directly from the hydrodealkylation of *m*-cresol, but rather includes transalkylation to other aromatics [44,45]. Alternatively, the role of a surface pool of condensed species can be considered. Due to the presence of strong acid sites, HMFI promotes the formation of the surface pool. However, the restricted pore structure of MFI would tend to reduce the size of this pool, and a smaller carbonaceous pool would lead to a lower extent of C—C bond formation. As a result, a higher selectivity to phenol, evolved from the surface during decomposition, should be expected on HMFI compared to HBEA, as shown in Table 4.

5. Conclusions

Ga-modified H-Beta (Ga/HBEA) zeolites are effective catalysts for the hydrodeoxygenation of *m*-cresol. The main conclusions of this study can be summarized as follows:

- The main products observed from *m*-cresol are toluene, benzene, and xylene. In addition, phenol, oxygenated, and bicyclic compounds are also formed. The presence of these products suggests that the formation of a "surface pool" of oxygenated intermediates may play a role in the reaction pathway.
- The pulse-mode experiments show that *m*-cresol is readily trapped inside the zeolite. These trapped species can undergo several reaction paths, as follows:
  a. Condensation to (deactivating) heavier products.
  b. Decomposition to phenol and aromatics.
  c. Hydrogenolysis of trapped products as well as of some of the larger molecular aggregates that have started to condense.

The last path, (c), is greatly accelerated in the presence of Ga and H_2 in the gas phase. Under these conditions, path (a) is much less predominant, so deactivation is slow.

Path (b) occurs even in the absence of H_2, but in that case, path (a) dominates, leading to a fast deactivation. Reactions in He or those in H_2, but without Ga (in the gas phase or the surface), show severe deactivation.

- The continuous-flow-mode experiments show that without H_2 in the feed, the hydrogenolysis activity is rapidly depleted. However, the BrØnsted sites of the zeolite are still active for generating the surface pool of condensation products as well as for the decomposition of these deposits, but not for deoxygenation, so mainly oxygenated compounds are produced. Also, it is observed that the lack of hydrogenolysis activity in the absence of H_2 leads to a rapid catalyst deactivation.
- By contrast, the presence of H_2 in the feed greatly enhances the deoxygenation activity, particularly on the Ga/HBEA catalysts, being significantly lower on Ga/HMFI and almost negligible on Ga/SiO_2. While the former is due to steric constraints of the pore structure, the latter is due to the inability of the support to stabilize well-dispersed Ga species, which under H_2 are the active sites for hydrogenolysis.

Acknowledgments

This research was supported by NSF EPSCoR (Grant 0814361) and DoE EPSCOR (Grant DE-SC0004600). One of the authors (A.A.) is grateful for a financial support from the Thailand Research Fund through the Royal Golden Jubilee Ph.D. Program (Grant No. PHD/0213/2548).

References

[1] A.J. Ragauskas, C.K. Williams, B.H. Davison, G. Britovsek, J. Cairney, A. Eckert, W.J. Frederick Jr., J.P. Hallet, D.J. Leak, C.H. Liotta, J.R. Mielenz, R. Murphy, R. Templer, T. Tschaplinski, Science 311 (2006) 484–489.
[2] S.E. Koonin, Science 311 (2006) 435.
[3] G.W. Huber, S. Iborra, A. Corma, Chem. Rev. 106 (2006) 4044–4098.
[4] A. Corma, S. Iborra, A. Velty, Chem. Rev. 107 (2007) 2411–2502.
[5] G.W. Huber, A. Corma, Angew. Chem. Int. Ed. 46 (2007) 7184–7201.
[6] L.R. Lynd, J.H. Cushman, R.J. Nichols, C.E. Wyman, Science 251 (1991) 1318–1323.
[7] C.E. Wyman, Appl. Biochem. Biotechnol. 45–46 (1994) 897–915.
[8] D. Mohan, C.U. Pittman Jr., P.H. Steele, Energy Fuels 20 (2006) 848–889.
[9] S. Czernik, A.V. Bridgwater, Energy Fuels 18 (2004) 590–598.
[10] E. Furimsky, Appl. Catal. A: Gen. 199 (2000) 147–190.
[11] Y.H.E. Sheu, R.G. Anthony, E.J. Soltes, Fuel Process. Technol. 19 (1988) 31–50.
[12] T. Sooknoi, T. Danuthai, L.L. Lobban, R.G. Mallinson, D.E. Resasco, J. Catal. 258 (2008) 199–209.
[13] P.M. Arvela, I. Kubickova, M. Snare, K. Eranen, D.Y. Murzin, Energy Fuels 21 (2007) 30–41.
[14] M. Snare, I. Kubickova, P.M. Arvela, D. Chichova, K. Eranen, D.Y. Murzin, Fuel 87 (2008) 933–945.
[15] E. Furimsky, Appl. Catal. A 199 (2000) 147–190.
[16] A. Saadi, R. Merabti, Z. Rassoul, M.M. Bettahar, J. Mol. Catal. A 253 (2006) 79–85.

[17] G.F. Santori, M.L. Casella, O.A. Ferretti, J. Mol. Catal. A 186 (2002) 223–239.
[18] P. Dana, Z. Petr, B. Martina, C. Libor, C. Jiri, Appl. Catal. A 332 (2007) 56–64.
[19] A. Saadi, Z. Rassoul, M.M. Bettahar, J. Mol. Catal. A 164 (2000) 205–216.
[20] J.A. Biscardi, E. Iglesia, Catal. Today 31 (1996) 207–231.
[21] G.J. Buckles, G.J. Hutchings, Catal. Today 31 (1996) 233–246.
[22] V.I. Hart, M.B. Bryant, L.G. Butler, X. Wu, K.M. Dooley, Catal. Lett. 53 (1998) 111–118.
[23] B.S. Kwak, W.M.H. Sachtler, W.O. Haag, J. Catal. 149 (1994) 465–473.
[24] B.S. Kwak, W.M.H. Sachtler, J. Catal. 145 (1994) 456–463.
[25] A. Montes, G. Giannetto, Appl. Catal. A 197 (2000) 31–39.
[26] P. Meriaudeau, C. Naccache, J. Catal. 157 (1995) 283–288.
[27] P. Meriaudeau, G. Sapaly, G. Wicker, C. Naccache, Catal. Lett. 27 (1994) 143–148.
[28] G.L. Price, V. Kanazirev, J. Catal. 126 (1990) 267–278.
[29] V. Kanazirev, G.L. Price, K.M. Dooley, Stud. Surf. Sci. Catal. 69 (1991) 277–285.
[30] V.B. Kazansky, I.R. Subbotina, R.A. van Santen, E.J.M. Hensen, J. Catal. 227 (2004) 263–269.
[31] A. Ausavasukhi, T. Sooknoi, D.E. Resasco, J. Catal 268 (I) (2009) 68–78.
[32] Z. Ji-Lu, J. Anal. Appl. Pyrol. 80 (2007) 30–35.
[33] T.J. Gricus Kofke, R.J. Gorte, G.T. Kokotailo, W.E. Farneth, J. Catal. 115 (1989) 265–272.
[34] I. Nowak, J. Quartararo, E.G. Derouane, J.C. Vedrine, Appl. Catal. A 251 (2003) 107–120.
[35] P. Meriaudeau, C. Naccache, Appl. Catal. 73 (1991) L13–L18.
[36] S. Svelle, P.O. Rønning, S. Kolboe, J. Catal. 224 (2004) 115–123.
[37] F.C. Patcas, J. Catal. 231 (2005) 194–200.
[38] M. Bjørgen, U. Olsbye, D. Petersen, S. Kolboe, J. Catal. 221 (2004) 1–10.
[39] M. Seiler, W. Wang, A. Buchholz, M. Hunger, Catal. Lett. 88 (2003) 187–191.
[40] W. Song, H. Fu, J.F. Haw, J. Am. Chem. Soc. 123 (2001) 4749–4754.
[41] N.R. Meshram, S.G. Hegde, S.B. Kulkarni, P. Ratnasamy, Appl. Catal. 8 (1983) 359–367.
[42] V. Mavrodinova, M. Popova, Catal. Commun. 6 (2005) 247–252.
[43] E. Iglesia, J.E. Baumgartner, G.L. Price, J. Catal. 134 (1992) 549–571.
[44] Xinli. Zhu, Richard G. Mallinson, Daniel E. Resasco, Appl. Catal. A 379 (2010) 172–181.
[45] X. Zhu, L.L. Lobban, R.G. Mallinson, D.E. Resasco, J. Catal. 281 (2011) 21–29.
[46] K.M. Dooley, C. Chang, G.L. Price, Appl. Catal. A 84 (1992) 17–30.
[47] G.D. Meitzner, E. Iglesia, J.E. Baumgartner, E.S. Huang, J. Catal. 140 (1993) 209–225.
[48] G.S. Pokrovski, J. Schott, J.L. Hazemann, F. Farges, O.S. Pokrovsky, GeoChimi. Cosmochimi. Acta. 66 (2002) 4203–4220.
[49] E.S. Shpiro, D.P. Shevchenko, O.P. Tkachenko, R.V. Dmitriev, Appl. Catal. 107 (1994) 147–164.
[50] T. Prasomsri, R.E. Galiasso-Tailleur, W.E. Alvarez, T. Sooknoi, D.E. Resasco, Appl. Catal. A 389 (2010) 140–146.
[51] T. Prasomsri, A.T. To, S. Crossley, W.E. Alvarez, D.E. Resasco, Appl. Catal. B: Environ. 106 (2011) 204–211.